Halupka, K. J., C. J. Abbott, Y. T. Wong, S. L. Cloherty, D. B. Grayden, A. N. Burkitt, E. N. Sergeev, C. D. Luu, A. Brandli, P. J. Allen, H. Meffin, and M. N. Shivdasani. 2017. Neural Responses to Multielectrode Stimulation of Healthy and Degenerate Retina. *Investigative Ophthalmology & Visual Science*. **58**(9): 3770-84.

Neural Responses to Multielectrode Stimulation of Healthy and Degenerate Retina

Kerry J. Halupka,[1–3] Carla J. Abbott,[4] Yan T. Wong,[5,6] Shaun L. Cloherty,[5,7] David B. Grayden,[1,3,8] Anthony N. Burkitt,[1,3] Evgeni N. Sergeev,[1] Chi D. Luu,[4] Alice Brandli,[4] Penelope J. Allen,[4] Hamish Meffin,[7,9] and Mohit N. Shivdasani[3,10]

[1]NeuroEngineering Laboratory, Department of Biomedical Engineering, The University of Melbourne, Victoria, Australia
[2]Data61, Commonwealth Scientific and Industrial Research Organisation (CSIRO), New South Wales, Australia
[3]Bionics Institute, East Melbourne, Victoria, Australia
[4]Centre for Eye Research Australia, Royal Victorian Eye and Ear Hospital; Department of Surgery (Ophthalmology), The University of Melbourne, Victoria, Australia
[5]Department of Physiology, Monash University, Victoria, Australia
[6]Department of Electrical and Computer Systems Engineering, Monash University, Victoria, Australia
[7]National Vision Research Institute, Australian College of Optometry, Victoria, Australia
[8]Centre for Neural Engineering, The University of Melbourne, Victoria, Australia
[9]Australian Research Council Centre of Excellence for Integrative Brain Function, Department of Optometry and Vision Sciences, The University of Melbourne, Melbourne, Victoria, Australia
[10]Department of Medical Bionics, The University of Melbourne, Victoria, Australia

Correspondence: Mohit N. Shivdasani, Bionics Institute, 384-388 Albert Street, East Melbourne, VIC 3002, Australia; mshivdasani@bionicsinstitute.org.

Submitted: December 13, 2016
Accepted: June 2, 2017

Citation: Halupka KJ, Abbott CJ, Wong YT, et al. Neural responses to multielectrode stimulation of healthy and degenerate retina. *Invest Ophthalmol Vis Sci*. 2017;58:3770–3784. DOI: 10.1167/iovs.16-21290

Purpose. Simultaneous stimulation of multiple retinal electrodes in normally sighted animals shows promise in improving the resolution of retinal prostheses. However, the effects of simultaneous stimulation on degenerate retinae remain unknown. Therefore, we investigated the characteristics of cortical responses to multielectrode stimulation of the degenerate retina.

Methods. Four adult cats were bilaterally implanted with retinal electrode arrays in the suprachoroidal space after unilateral adenosine triphosphate (ATP)–induced retinal photoreceptor degeneration. Functional and structural changes were characterized by using electroretinogram a-wave amplitude and optical coherence tomography. Multiunit activity was recorded from both hemispheres of the visual cortex. Responses to single- and multielectrode stimulation of the ATP-injected and fellow control eyes were characterized and compared.

Results. The retinae of ATP-injected eyes displayed structural and functional changes consistent with mid- to late-stage photoreceptor degeneration and remodeling. Responses to multielectrode stimulation of the ATP-injected eyes exhibited shortened latencies, lower saturated spike counts, and higher thresholds, compared to stimulation of the fellow control eyes. Electrical receptive field sizes were significantly larger in the ATP-injected eye than in the control eye, and positively correlated with the extent of degeneration.

Conclusions. Significant differences exist between cortical responses to stimulation of healthy and degenerate retinae. Our results highlight the importance of using a retinal degeneration model when evaluating the efficacy of novel stimulation paradigms.

Keywords: retinal prosthesis, retinal degeneration, in vivo electrophysiology, electrical stimulation, computational modeling

Retinitis pigmentosa is a leading degenerative disease of the visual system that causes photoreceptor loss and eventual blindness.[1,2] Treatments for these conditions include retinal prostheses,[3–5] cortical prostheses,[6] optogenetic therapies,[7] and stem-cell treatments.[8] This work focuses on retinal prostheses, which provide a sense of vision by electrically stimulating surviving neurons of the retina. Although clinical trials have shown that retinal prostheses can elicit useful percepts,[3,9–12] spatial resolution is a limiting factor, particularly for implants located far from the target cells such as with the suprachoroidal approach.[3,13]

Animal studies suggest that spatial resolution and numbers of distinct percepts can be improved with appropriate stimulation strategies.[14–18] Such strategies apply simultaneous stimulation across multiple electrodes, with interactions between electrodes altering the electrical field at the retina to reduce the spread of activation[15,16] ("current focusing") or activate groups of cells between electrodes[14] ("current steering"). However, stimulation strategies demonstrated in healthy retinae cannot necessarily be extrapolated to degenerate retinae.[19–23] Consequently, the large body of knowledge derived from animal studies is difficult to translate into clinical

practice. This highlights a need to comprehensively evaluate the responses of degenerate retinae to electrical stimulation.[24]

Studies in blind human patients have investigated concurrent simulation of pairs,[4,25,26] rows,[5,27–29] or blocks of several electrodes.[30–32] The evoked percepts from these types of stimulation strategies have been reported to be variable across trials and patients, suffering from low predictability and dissimilarities between studies.[33] It is unknown whether stimulation strategies that successfully focus or steer current in healthy retinae can provide meaningful improvements when applied to degenerate retinae.

In this study, we investigated cortical responses to simultaneous stimulation of multiple retinal electrodes in a feline model with unilateral adenosine triphosphate (ATP)–induced photoreceptor degeneration. This work builds upon a previous study that shows that glial changes in the ATP-injected retina significantly influence the efficacy of single-electrode stimulation.[24] The cat visual system has long been studied as an analogue for human vision,[34] making the photoreceptor degeneration model ideal for the development of retinal prostheses.[24,35,36] The similarity in size of the cat eye to the human eye also enables clinically relevant electrode size and positioning, with a similar level of photoreceptor degeneration and remodeling to that seen in humans with retinitis pigmentosa.[36] Blindness was induced by intravitreal injection of ATP in a single eye, allowing comparison of healthy and degenerate retinae in the same animal.[24] As such, the ATP-injected cat model is ideal for investigating cortical responses to simultaneous stimulation of multiple retinal electrodes, which previous in vivo studies have not explored. As a first step toward understanding the reasons behind the variability seen in patients and to determine how current focusing and steering can be applied to degenerate retinae effectively, the aim of this study was to examine how loss of photoreceptors influences the cortical responses to multielectrode stimulation.

Methods

This study used bilateral implantation of retinal electrode arrays in the suprachoroidal space of adult cats with unilateral ATP-induced retinal degeneration. Neural responses were recorded from both hemispheres of the visual cortex. Responses to single- and multielectrode stimulation of the ATP-injected and fellow control eyes were characterized and compared. Treatment of animals complied with the Association for Research in Vision and Ophthalmology Statement for Use of Animals in Ophthalmic and Vision Research, and the National Health and Medical Research Council's Australian Code of Practice for the Care and Use of Animals for Scientific Purposes (2013) and the Prevention of Cruelty to Animals Act (1986 and amendments). The study was approved by the Bionics Institute Animal Research and Ethics Committee (Project No. 14/304AB).

Intraocular Injection of ATP and Clinical Assessments

Five adult cats were used in this study; however, one animal developed a large retinal detachment 2 weeks after the ATP injection and was not used further. Anesthesia for both ATP injections and clinical assessments was induced via a subcutaneous injection containing ketamine (20 mg/kg, Ilium Ketamil; Troy Laboratories, Glendenning, NSW, Australia) and xylazine (2 mg/kg, Ilium Xylazil-20; Troy Laboratories). Pupils were dilated with 1% tropicamide and 2.5% phenylephrine hydrochloride, corneal lubrication was provided with HPMC PAA gel (Alcon, Fort Worth, TX, USA). Hartmann's solution (2.5 mL/kg/h) was given subcutaneously to prevent dehydration and aid recovery. The procedure for inducing unilateral retinal degeneration has been previously described in detail.[24,35,37,38] One eye was injected with a 200 μL solution of three parts sterile saline (0.9% NaCl) and one part Dexamethasone (4 mg/mL), containing approximately 0.2 M (11 mM vitreous concentration) ATP disodium salt (Sigma-Aldrich Corp., St. Louis, MO, USA) to induce photoreceptor degeneration. The fellow eye was a noninjected control. Multiple (2–3) ATP injections were required to induce a sufficient level of degeneration at the area centralis. Clinical assessments were performed to monitor the course of degeneration at approximately 2 weeks after each injection, approximately 4 weeks before the endpoint, and at the endpoint. The experimental endpoint (surgical implantation and acute electrophysiology) was a minimum of 12 weeks (15_401B: 14 weeks, 15_402B: 23 weeks, 15_403B: 16 weeks, 16_405B: 16 weeks) after the final ATP injection in order to maximize photoreceptor degeneration.[35]

Clinical assessments of retinal structure and function were performed as described elsewhere.[35] Under anesthesia, a full-field flash electroretinogram (ERG, Espion; Diagnosys LLC, Lowell, MA, USA) was used to record the retinal response to stimulus intensities from 0.001 to 10 cd.s/m^2 after 20 minutes of dark-adaptation; however, only the combined rod–cone maximal ERG response (10 cd.s/m^2) is reported. The a-wave amplitude was used to measure photoreceptor function. Note that the final ERG was taken approximately 4 weeks before endpoint, as the ERG response could not be elicited immediately after surgery. Spectral-domain optical coherence tomography (SD-OCT, Spectralis HRA+OCT; Heidelberg Engineering GmbH, Heidelberg, Germany) and color fundus photography (TRC-50Dx; Topcon Medical Systems, Oakland, NJ, USA) were used to assess retinal structure. Line scans were used to confirm photoreceptor dropout at the area centralis and to ensure the retinal array was placed at an area of degeneration, since the ATP degeneration model does not produce uniform photoreceptor loss. Sufficient photoreceptor degeneration was classified as at least 50% reduction in ERG a-wave amplitude along with accompanying outer retina dropout at the area centralis, assessed by SD-OCT. As described previously,[35] retinal thickness was defined as the distance between the inner limiting membrane to the border of the retinal pigment epithelium (RPE)/tapetum, inner retinal thickness as the distance between the inner limiting membrane to the inner nuclear layer/outer plexiform layer boundary, and outer retinal thickness as the distance between the inner nuclear layer/outer plexiform layer boundary and the RPE/tapetum boundary. These thicknesses were measured at 20 locations regularly spaced over the tip to central parts of the array in both ATP and fellow control eyes at the final assessment immediately after array implantation. In one animal (15_401B), measures were taken for locations immediately adjacent (nasal) to the array tip owing to the array being located too far temporally for the SD-OCT. In addition, the retina to electrode distance (RTED) was defined from the center of each identified electrode to the border of the RPE/tapetum layers, and averaged across all identified electrodes and animals (since the RTED is the same for both the ATP-injected and fellow control eyes). Two-way ANOVA with Sidak's multiple comparison post test was performed on the SD-OCT thickness data with GraphPad Prism V7 software (GraphPad, San Diego, CA, USA).

Acute Electrophysiology Experiment Setup

Cats were premedicated with a dose of Medetomidine (0.012 mg/kg, intramuscular [IM]), ketamine (8 mg/kg, IM), and

methadone (0.4 mg/kg, IM). Anesthesia was induced and maintained with an intravenous infusion of Propofol (24 mg/kg). A solution of Hartmann's and Methadone (0.25 mL of 10 mg/mL Methadone in 250 mL compound sodium lactate, 0.05 mg/kg/h) was also delivered intravenously. A tracheotomy was performed and the animal was ventilated with 100% oxygen (20–25 breaths/min) (model 6025; Ugo Basile, Monvalle, VA, Italy). Dexamethasone (0.3 mg/kg, IM) and Clavulox (10 mg/kg, subcutaneous) injections were given daily. Core body temperature was maintained at 37°C and physiological indicators, including expired CO_2, O_2 saturation, heart rate, and blood pressure, were continuously monitored throughout the experiment. The experiments were typically conducted over 3 to 4 days, after which the animal was killed, by using an overdose of intravenous sodium pentobarbitone (60 mg/kg; Troy Laboratories).

Stimulating Electrode Array

Once anesthetized, animals were bilaterally implanted with suprachoroidal electrode arrays by using a previously described surgical procedure.[39] The arrays consisted of flexible medical-grade silicone substrates with 7 rows × 6 columns of platinum electrodes (600-μm diameter, 1-mm pitch) and a helical platinum–iridium cable.[40] A lateral canthotomy was performed and the choroid was exposed via a scleral incision. A pocket was created between the sclera and choroid into which the electrode array was inserted and sutured in place.[40]

Cortical Electrophysiology

Following suprachoroidal array implantation, both hemispheres of the visual cortex were exposed with a bilateral craniotomy and penetrating microelectrode arrays (6 × 10 channels, 1-mm length, 400-μm spacing; Blackrock Microsystems, Salt Lake City, UT, USA) were implanted. Optimal microelectrode array positions were determined by first recording evoked potentials (EPs) from the cortical surface in response to retinal stimulation.[14,17]

Neural signals were sampled at 30 kHz (Cerebus Neural Processing System; Blackrock Microsystems) with offline stimulus artifact removal[17,39,41] and band-pass filtering (third-order Butterworth filter, 300–5000 Hz). Multiunit spiking activity (MUA) was detected by threshold crossings (at four times the root-mean-square of a 60-second moving time window).

We analyzed the period from 3 to 20 ms post stimulus, which is considered to include spikes as a result of both direct stimulation of retinal ganglion cells (RGCs) and indirect activation of the inner retina.[42] The spontaneous spiking rate on each channel in the 500 ms before each stimulus was subtracted to account for variation in the stimulus-independent activity.

Visual Stimulation

Cortical responses to flashes (1.5 cd·s/m^2 with a duration of 10 μs at 1 Hz) were delivered with a FLYSYS FlashLamp System (Tucker-Davis Technologies, Alachua, FL, USA) with the lamp guide placed approximately 2.5 cm in front of each eye individually (with a patch covering the fellow eye).

Single-Electrode Electrical Stimuli

All electrical stimuli consisted of charge-balanced biphasic current pulses with 1-ms phase width and 25-μs interphase gap at a 1-Hz presentation rate. Electrical stimulation was provided by a multichannel stimulator (RZ2 base station and IZ2 multichannel stimulator; Tucker Davis Technologies) commanded by a custom-made MATLAB (version 2014b; MathWorks, Inc., Natick, MA, USA) interface. Electrodes were first individually stimulated with cathodic-first pulses, 0- to 750-μA stimulus amplitude, in 50-μA steps, with 10 repetitions of each amplitude. For each stimulating electrode/recording channel combination, a sigmoid curve was fitted to the mean spike-rate (3- to 20-ms window) as a function of stimulation amplitude. A P50 current of the sigmoid was calculated as the stimulus amplitude at which the spike rate reached 50% of the maximum.[17] For each stimulating electrode, the lowest P50 current across all recording channels was used in the generation of the multielectrode simultaneous stimuli.

Multielectrode Simultaneous Electrical Stimulation

Multielectrode stimulation consisted of temporally sparse (1 Hz), spatially white electrical pulse patterns delivered simultaneously across the stimulating electrodes in each eye separately. This form of stimulation is suitable for estimating several key parameters of the cortical response via fitting to a linear–nonlinear model as described previously[43] and summarized below. The stimulus amplitude for each electrode was sampled from a zero-mean Gaussian distribution, with the standard deviation equal to the P50 current for that electrode. For stimulating electrodes where a sigmoid could not be reliably fitted to responses to single-electrode stimulation, and therefore a P50 current could not be determined, the standard deviation was scaled by the average P50 current on all other electrodes. The zero mean of the Gaussian distribution meant that a mix of cathodic-first and anodic-first waveforms were presented in each pattern (negative amplitudes as cathodic-first). A total of 3150 multielectrode stimulation patterns were generated separately for each eye in all experiments. Since the distribution of stimulus amplitudes for each electrode depended on the threshold for that electrode, the 3150 patterns presented to the healthy retina were different from those presented to the degenerate retina. Each pattern was presented eight times and the responses averaged.

Linear–Nonlinear Model

To characterize differences in cortical responses to multielectrode stimulation in both the healthy and degenerate retinae, a linear–nonlinear model was fitted to the Gaussian white noise stimulation responses.[43–45] This model provides information about the response of each cortical recording site to stimulation of multiple electrodes, including which electrodes significantly affect each channel, and the nonlinear characteristics, such as response thresholds and saturation levels. The model comprises two spatial linear filters (V_P and V_N), followed by two parallel static nonlinearities (g_P and g_N) for each recording channel. An estimate of the spike count (R_{est}) in response to a stimulus vector at time t (s_t) is given by

$$R_{est} = g_P(s_t^{tr} V_P) + g_N(s_t^{tr} V_N), \quad (1)$$

where tr is the matrix transpose. Two filters were required to account for net anodic-first (V_P and g_P) or net cathodic-first (V_N and g_N) stimulation (where net anodic-first means that the sum of the biphasic pulses across all electrodes, weighted by V_P, is positive). The spatial linear filters, recovered by using spike-triggered covariance analysis and normalized by dividing by their L-2 norm, serve to project the high-dimensional stimulus ($M = 42$ electrodes) into a single-dimensional subspace, termed the "generator signal" subspace. The spatial linear filters can be interpreted as electrical receptive fields (ERFs) of a population of neurons at each cortical recording channel.[46]

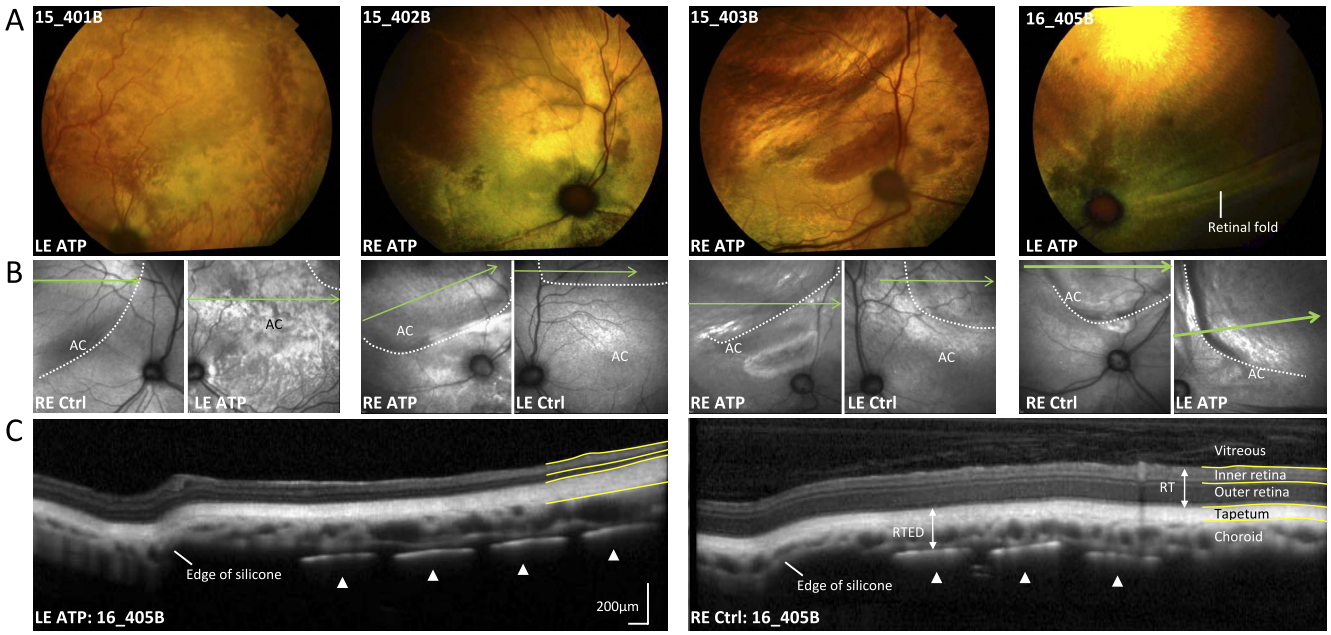

Figure 1. **(A)** Color fundus photographs in the ATP-injected eye for each subject, showing mottled pigmentation consistent with widespread but variable photoreceptor degeneration across the retina. Subject numbers are shown on each panel. **(B)** Infrared images from both ATP-injected and healthy fellow control eyes for each subject, indicating implant position (*dotted lines*) relative to the area centralis (AC). The *bold green arrows* in 16_405B indicate the position of the SD-OCT scans in **(C)**. **(C)** Representative SD-OCT images from both eyes of 16_405B demonstrate thinning of the outer retina in the ATP-injected eye. There was variability in outer retinal thinning across the retina, with the ATP-injected eye in this example showing greater thinning temporally (*right side* of image). The locations of electrodes are indicated by *arrowheads*. Total retinal thickness (RT) and retina to electrode distances (RTEDs) are shown with *arrows*. *Yellow boundaries* show the segmentation of the boundaries between the vitreous, inner retina, outer retina, tapetum, and the choroid. ATP, ATP-injected eye; Ctrl, fellow control eye; LE, left eye; RE, right eye.

To determine the significance of each electrode's contribution to the ERF, a control distribution was generated for both V_P and V_N by repeating the fitting procedure 1000 times on randomly time-shifted responses. Electrodes with linear filter values larger than the root-mean-square of the randomly generated distribution were considered significant. The size of each ERF is then given by

$$D_P = \frac{\sum_{j=1}^{M} v_j^P d_j}{\sum_{j=1}^{M} v_j^P} \quad (2)$$

$$D_N = \frac{\sum_{j=1}^{M} v_j^N d_j}{\sum_{j=1}^{M} v_j^N}, \quad (3)$$

where d_j is the distance of each electrode j to the center of mass of the significant electrodes and v_j^P and v_j^N are the weights given by V_P and V_N, respectively. ERF sizes were converted to degrees of visual angle by using a 4.4-deg/mm conversion factor for the cat eye.[47]

The static nonlinearities, which account for nonlinear response characteristics such as thresholds and saturation, were recovered by projecting the stimuli onto the linear filters to recover generator signal values $x_P = s_t^{tr} V_P$ and $x_N = s_t^{tr} V_N$, then fitting a sigmoidal function to the binned generator signal values and their respective responses (spike count averaged over repeated trials). The static nonlinearities g_P and g_N are fitted by using the logistic equations

$$g_P(x_P) = \frac{y_P}{1 + \exp(-b_P(x_P - a_P))} \quad (4)$$

$$g_N(x_N) = y_N - \frac{y_N}{1 + \exp(-b_N(x_N - a_N))}, \quad (5)$$

where y_P and y_N are the saturation spiking levels in response to net anodic-first and net cathodic-first stimulation, respectively; a_P and a_N are the P50 levels; and b_P and b_N represent the slopes at P50 of each sigmoid. The summation of the outputs of these sigmoid functions provided a predicted response (R_{est}) for each cortical channel for any stimulus vector, as defined in Equation 1.

To determine the accuracy of the model in characterizing cortical responses, we compared the responses predicted by the fitted model to the actual recorded responses for all 3150 multielectrode patterns. Only channels that exhibited a coefficient of determination (r^2) of at least 0.5 were considered in further analyses.

Results

Arrays Were Positioned Over ATP-Induced Photoreceptor Degenerated Regions

ATP injections caused photoreceptor degeneration over a period of >12 weeks unilaterally in four subjects (Fig. 1), consistent with previous publications.[35,36] The color fundus photographs (Fig. 1A) from the ATP-injected eyes show widespread mottled pigmentation indicating broad but variable degeneration both across an individual retina and between subjects. Additionally, there was a marked attenuation of inner retinal vessels in 16_405B, likely occurring in response to extensive photoreceptor degeneration.[36] The implant position relative to the area centralis (Fig. 1B) was asymmetric between eyes in 15_401B and 15_402B, with the array in the right eye underlying the area centralis and that in the left eye being >4 disc diameters (>6 mm) from the area centralis. The other two subjects (15_403B and 16_405B) had implants positioned near the area centralis in both eyes, although the right eye implant

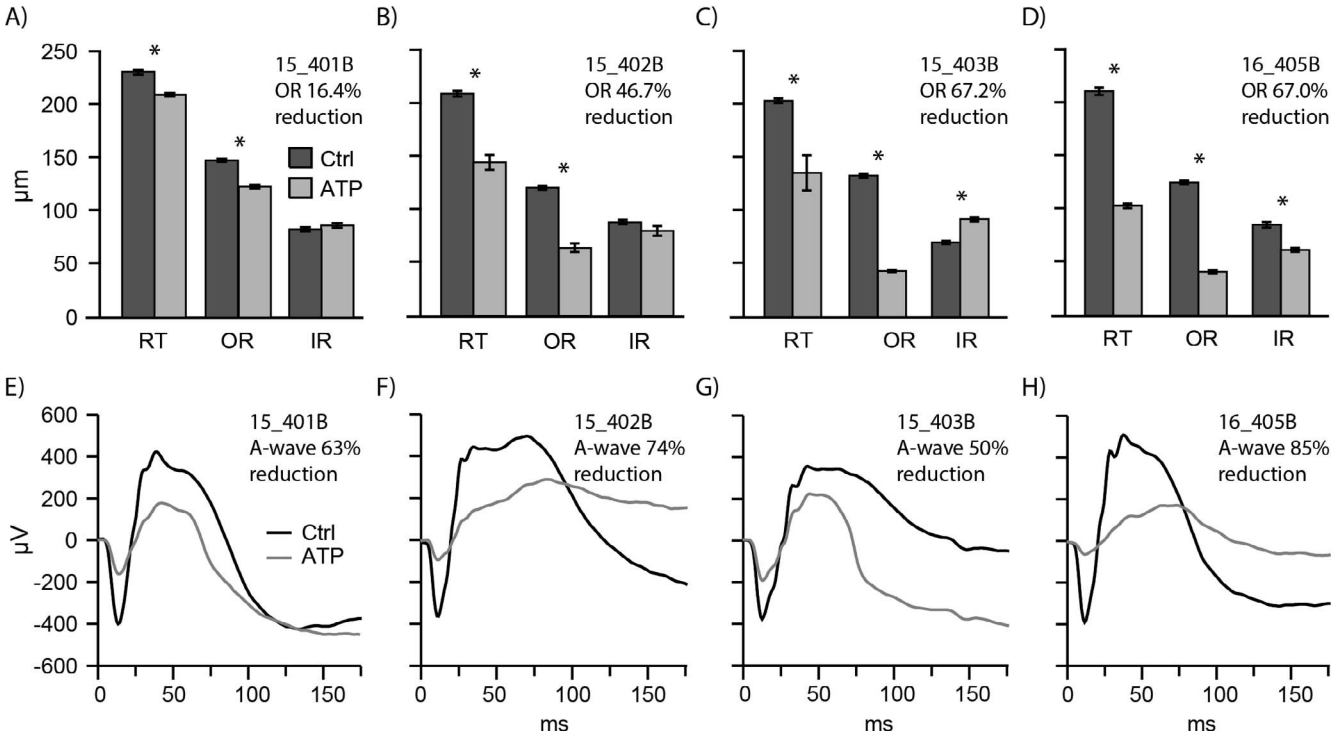

Figure 2. (**A–D**) SD-OCT scans showed a reduction in total RT by 9% to 50%, predominantly due to a decrease in outer retinal thickness (OR; 16%–67%) in ATP-injected eyes as compared to healthy fellow eyes. Inner retinal thickness (IR) showed a trend for mild thinning in two subjects (15_402B, 16_405B) and a trend for mild thickening in two subjects (15_401B, 15_403B). Measures over the array could not be attained for the ATP-injected eye of subject 15_401B, and therefore the measures shown are from the retinal area adjacent to the array for the ATP-injected eye. *Error bars* indicate mean ± SEM, markers (*) indicate $P < 0.0001$. (**E–H**) Combined rod–cone ERG responses (10 cd.s/m^2) in each subject showed a global reduction in the a-wave amplitude (photoreceptor function) in all ATP-injected eyes by 50% to 85% relative to the healthy fellow eyes.

positions were relatively nasal compared to the left eye implant positions. There was outer retinal degeneration and thinning overlying electrodes as seen in the representative SD-OCT scan shown in Figure 1C, although regional variability of degeneration is evident (thinner retina temporally [right side of scan] in the ATP eye). The array was positioned too far temporally in 15_401B to obtain images of retina overlying the array, although since the degeneration appears widespread (Fig. 1A), there likely was degeneration overlying the array in this subject as well.

Over the array, there was total retinal thinning (9%–51%, all $P < 0.0001$, 2-way ANOVA with Sidak multiple comparison test) evident in the ATP eye relative to the fellow control, which was predominantly due to thinning of the outer retina (16%–67%, all $P < 0.0001$) (Fig. 2A). In two subjects (15_401B, $P = 0.033$; 15_402B, $P = 0.42$) the inner retina was well conserved, while in one subject there was inner retinal thinning (16_405B, 28% thinning, $P < 0.0001$) and in one subject there was inner retinal thickening (15_403B, 31% thickening, $P < 0.0001$), most likely due to the presence of gliosis as shown previously.[24] The distance from the electrodes to the target cells (bipolar and ganglion cells) was estimated by combining the distance between the identified electrodes and the retina (mean ± SD: 359 ± 78 µm, $n = 62$ electrodes; RTED in Fig. 1C) with the retinal thickness data. This showed that, in the ATP-injected eye, the approximate distance to the bipolar cells was 430 µm, and 490 µm to the ganglion cells. In the fellow control eye, these distances were larger on average, at 490 and 550 µm, respectively.

The reduction in the a-wave of combined rod–cone ERG responses (10 cd.s/m^2) in all ATP-injected eyes relative to the healthy fellow eyes was 50% to 85% (Figs. 2E–H), indicating a significant global reduction in photoreceptor function. Animal 16_405B had the greatest photoreceptor degeneration by both structural and functional measures (Fig. 2), while the others were mixed as to whether the global functional deficit or localized structural deficit was more pronounced.

Cortical Responses to Electrical Stimulation of the Degenerate Retina Have Shorter Latencies

Following confirmation of sufficient unilateral photoreceptor degeneration, suprachoroidal stimulating arrays were bilaterally implanted. Additionally, two 60-channel recording arrays were implanted in each animal (480 implanted electrodes in total), but one channel in each experiment was deemed nonfunctioning before implantation. Therefore, cortical responses to single- and multielectrode stimulation of healthy and degenerate retinae were recorded on a total of 476 recording channels. Deterioration of the cortical response to visual stimulation of the blind eye was confirmed with light flashes to both eyes of each animal. Figure 3A shows a peristimulus time histogram (PSTH) of the MUA response to visual stimulation of the normal and blind eyes in 16_405B, smoothed with cubic interpolation. Clear early (photoreceptor mediated) and late (possibly due to cortical feedback) response peaks could be distinguished in the flash response from the normal eye ($P < 0.001$ both peaks before smoothing, rank sum test versus baseline with Bonferroni correction, 0–50 ms and 50- to 200-ms windows), while flashing the blind eye yielded no response above baseline for either peak ($P = 0.04$ and $P = 0.22$ for the early and late peaks, respectively; rank sum test with Bonferroni correction). All other animals also exhibited significant early and late response peaks from flashing the control eye ($P < 0.001$ for all comparisons). However, the

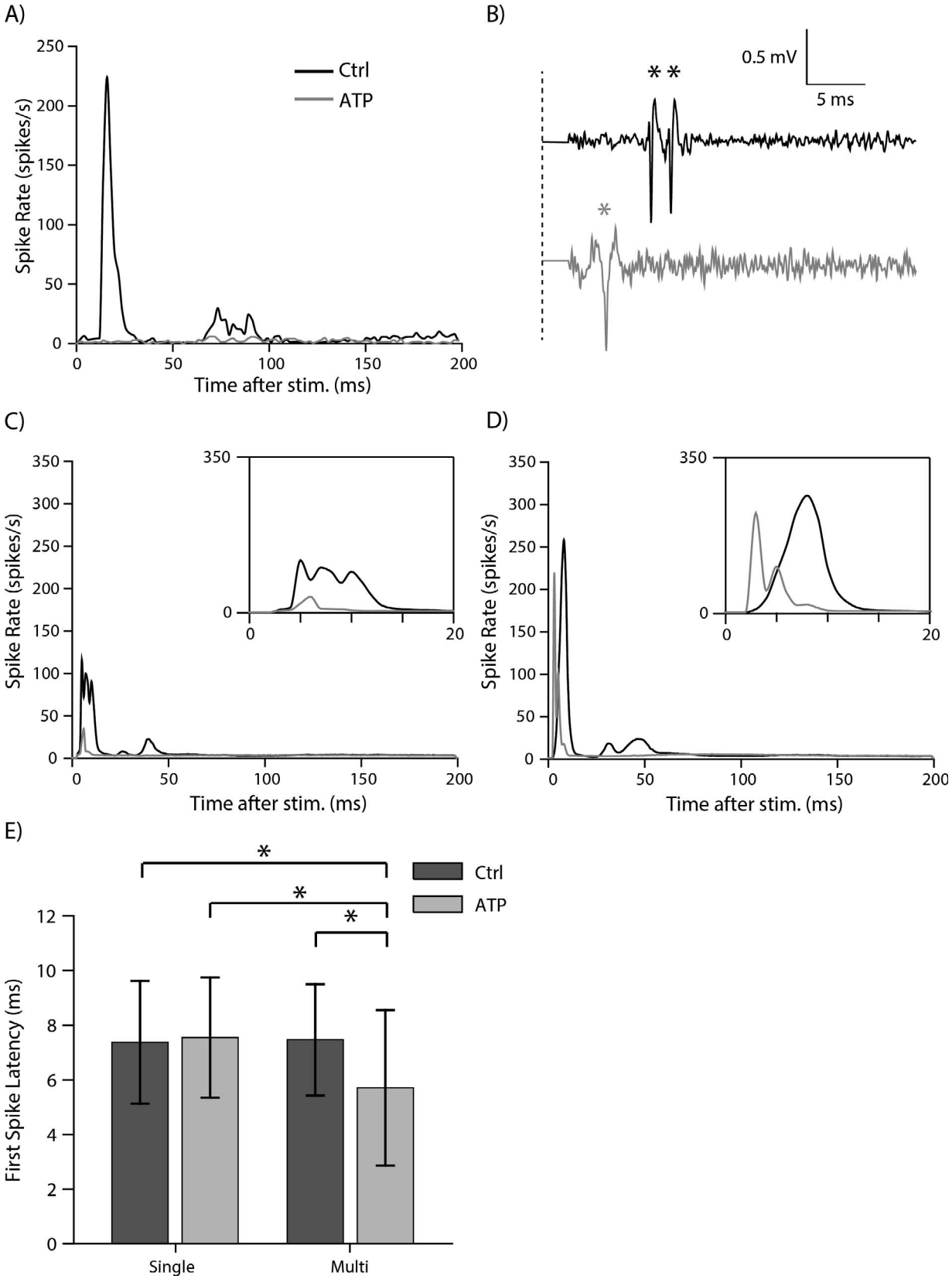

Figure 3. (**A**) PSTHs in response to flashes directed at ATP-injected eye (*gray line*) and fellow control eye (*black line*), averaged over all cortical channels and 10 repetitions, for 16_405B ($n = 120$ channels $\times$ 10 repetitions, bin width = 2 ms). Cubic interpolation was used to smooth all PSTHs. (**B**) Filtered trace on two recording channels from multielectrode stimulation showing spiking (indicated by *asterisks*). *Dashed line* indicates the beginning of the stimulus pulse, the electrical artifact at the beginning of the trace has been blanked, and is shown here replaced by a flat line. (**C**, **D**) Smoothed PSTHs of responses to (**C**) single-electrode and (**D**) multielectrode stimulation, averaged over all cortical sites and stimuli, in both the ATP-injected eye (*gray line*) and the fellow control eye (*black line*), in 16_405B. Inset panels show a close-up view of the time period 0 to 20 ms post stimulus. (**E**) First spike latency for cortical channels that exhibited at least one spike per trial averaged over all experiments. *Error bars* indicate mean $\pm$ SD, markers (*) indicate $P < 0.001$.

strengths of response of the ATP-injected eyes varied in significance, with significant early and late responses ($P < 0.001$ for all comparisons) recorded in the two animals that exhibited less pronounced photoreceptor degeneration (1 and 2). Neither response peak was significant in 15_402B with 74% degeneration ($P = 0.51$ and $P = 0.06$ for the early and late peaks, respectively).

Electrical stimulation of both degenerate and healthy retinae elicited robust MUA (Fig. 3B). PSTHs of responses to single-electrode stimulation (Fig. 3C) and multielectrode stimulation (Fig. 3D), collated over all stimulus levels and cortical channels, showed that both stimulus types were able to elicit early cortical responses within the first 20 ms regardless of retinal health ($P < 0.001$, rank sum test). For these early responses, firing rates were markedly different between healthy and degenerate retinae and between single- and multielectrode stimulation.

Late spiking components (>20 ms) to electrical stimulation, which are likely to be network mediated, were observed from stimulation of the healthy retina but were largely or completely absent when stimulating the degenerate retina (response significantly greater than baseline for single-electrode stimulation in 30- to 100-ms window: $P < 0.001$ healthy retina, $P = 0.14$ degenerate retina; for multielectrode stimulation: $P < 0.001$ healthy retina, $P = 0.06$ degenerate retina, rank sum test). Across the four animals, the early response was consistently significantly above baseline ($P < 0.001$ for both retinae and stimulus types, rank sum test) and late responses were not significant for stimulation of the degenerate retina ($P = 0.17$ for single-electrode stimulation, $P = 0.29$ for multielectrode stimulation, rank sum test).

For the population, the first spike latency averaged across all cortical channels that exhibited at least one spike per trial (Fig. 3E) was found to depend significantly on the interaction between stimulus type and retinal health status. In particular, multielectrode stimulation of the ATP-injected eye resulted in significantly shorter latencies than any other stimulus type/retina status combination ($P < 0.001$ for all comparisons, 2-way ANOVA with Bonferroni correction). This result was also present and significant for each animal individually ($P < 0.001$ for all comparisons). There was no significant difference between first spike latencies to single- versus multielectrode stimulation of the control eyes ($P = 0.12$, 2-way ANOVA with Bonferroni correction; Fig. 3E), or between single-electrode stimulation for either eye status ($P = 0.047$, 2-way ANOVA with Bonferroni correction). These results were also present in all animals individually, except for 16_405B with the greatest photoreceptor degeneration (85%) and largest retinal thinning (50%), which exhibited significantly shorter latencies to single-electrode stimulation of the ATP-injected eye than in the control eye ($P < 0.001$).

Retinal Degeneration Leads to Higher Cortical Thresholds and Lower Saturated Spike Rates

To more directly compare responses of single- and multielectrode stimulation, we converted both single- and multielectrode stimuli into a generator signal by projecting the stimuli onto the linear filters, defined by our linear–nonlinear model fitted to multielectrode stimulation responses (see Methods). We then plotted the responses as functions of this common generator signal to reveal nonlinear relationships (examples shown in Figs. 4A, 4B). Only cortical channels that responded to both multielectrode stimulation and at least one single electrode were included in this analysis (control eye: $n = 184$, ATP-injected eye: $n = 72$). For responses to single-electrode stimulation (dashed black lines), only the stimulating electrode eliciting the lowest P50 current for each channel was used in the comparison. Across the population, saturation spike levels (90% of sigmoid maximum), generator signal amplitudes at saturation (P90 generator current), and thresholds, defined as the generator signal value required to evoke a firing rate of at least 3 standard deviations above baseline, were compared. This definition of threshold (as opposed to a fixed point on the sigmoid) mitigated the impact of dynamic range differences observed between single- and multielectrode stimulation.

Population metrics indicated that multielectrode stimulation elicited significantly higher ($P < 0.001$, 2-way ANOVA with Bonferroni correction) saturated spike levels than single-electrode stimulation in the control (mean ± SD: single-electrode, 2.52 ± 1.04; multielectrode, 3.61 ± 1.15) and ATP-injected (mean ± SD: single-electrode, 1.81 ± 0.72; multielectrode, 2.61 ± 0.75) eyes (Fig. 4C). Furthermore, multielectrode stimulation of the healthy retina resulted in higher saturation levels than that of the degenerated retina ($P < 0.001$, 2-way ANOVA with Bonferroni correction; Fig. 4C). This result was generally consistent on an individual basis; however, 15_403B showed no significant difference between eyes for saturation responses to multielectrode stimulation ($P = 0.8$). 16_405B was the only animal for which single-electrode stimulation elicited higher saturated spike rates in the control eye than the degenerate eye ($P = 0.002$), with all others exhibiting no significant difference.

The amplitude of the generator signal value at which the saturated spike count was reached (P90 generator current) was significantly lower when stimulating the control (mean ± SD: single-electrode, 112.1 ± 57.6; multielectrode, 99.0 ± 45.6) versus the ATP-injected (mean ± SD: single-electrode, 177.9 ± 66.4; multielectrode, 185.3 ± 60.2) eyes ($P < 0.001$ for both single- and multielectrode stimulation, 2-way ANOVA with Bonferroni correction) on a population basis (Fig. 4D). No significant difference was observed between single- and multielectrode stimulation P90 generator currents for either the control ($P = 0.14$, 2-way ANOVA with Bonferroni correction) or the ATP-injected eye ($P = 1$, 2-way ANOVA with Bonferroni correction). Individual animal statistics were consistent with that of the population.

Multielectrode stimulation also resulted in significantly lower thresholds than single-electrode stimulation regardless of retinal health status (control eye: $P < 0.001$; ATP-injected eye: $P = 0.0019$, 2-way ANOVA with Bonferroni correction) on a population basis (Figs. 4E, 4F). Furthermore, stimulation of the control eye resulted in significantly lower thresholds than in the ATP-injected eye for both stimulus types (single-electrode: $P = 0.004$; multielectrode: $P = 0.002$). These results were generally consistent for most animals individually; however, 15_403B showed no significant threshold difference between eyes for either single-electrode stimulation ($P = 1$) or multielectrode stimulation ($P = 0.07$).

Retinal Degeneration Results in Increased Electrical Receptive Field Sizes

Interactions between electrodes during multielectrode stimulation mean that the activity of a particular cortical channel can be affected by subthreshold stimulation of distant electrodes, thereby possibly limiting resolution. This effect can be measured by the ERF size for each cortical channel. The linear filters of the linear–nonlinear model characterized by white noise stimulation can be interpreted as ERFs and indicate the relative strength of the effect of each stimulating electrode on a cortical site. Generally, ERFs were found to be spatially localized and roughly oval, with a central peak in electrode efficacy that diminished to negligible levels further from the center in both the control (Figs. 5A, 5B) and ATP-injected (Figs. 5C, 5D) eyes. However, ERFs were noticeably larger in the ATP-

Investigative Ophthalmology & Visual Science

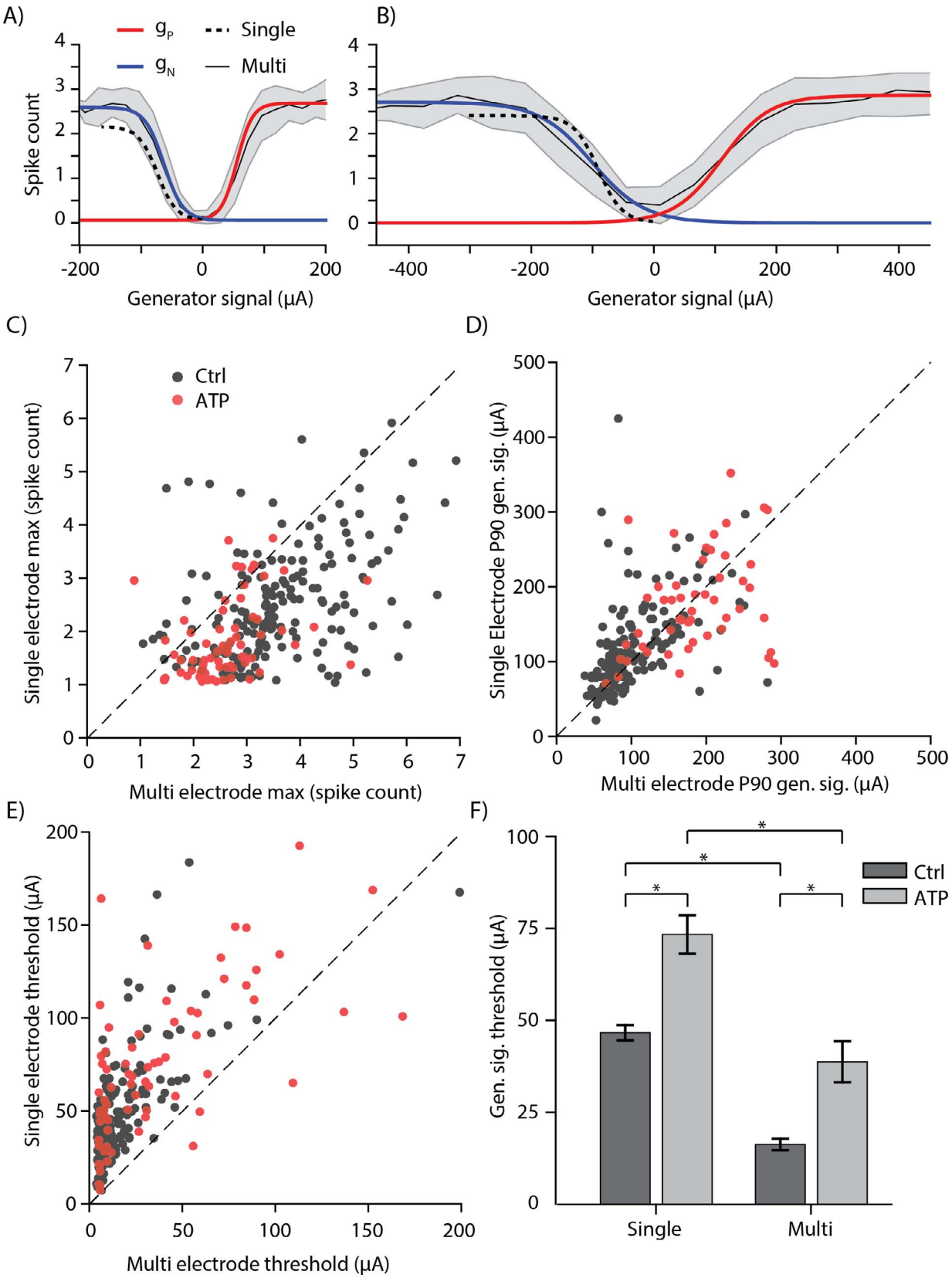

Figure 4. (**A**, **B**) Examples of multielectrode static nonlinearities g_N (*blue line*) and g_P (*red line*) for the control eye (**A**) and ATP-injected eye (**B**) for one cortical channel in 15_401B. *Solid black line* shows the average recorded response to each of the binned generator signal levels (mean ± SEM, shown in *gray*). *Dashed black line* shows the sigmoid fitted to responses to cathodic-phase-first single-electrode stimulation. Note that the *x*-axis scale is equal in both panels; however, the mean current amplitude used for the ATP-injected eye was higher owing to increased thresholds, resulting in an increased range in generator signal values. (**C**) Saturated spike count, (**D**) generator signal value at 90% of saturated spike count (P90), and (**E**) activation threshold (generator signal at 3 × standard deviation of baseline spike rate) for multielectrode stimulation versus single-electrode stimulation in response to stimulation of the control (*black markers*) and ATP-injected eyes (*red markers*) for all animals collated ($n = 184$ for control eye, $n = 72$ for ATP-injected eye). (**F**) Comparison of thresholds collated across experiments. Markers (*) indicate a 0.001 level of significance. *Error bars* indicate mean ± SE.

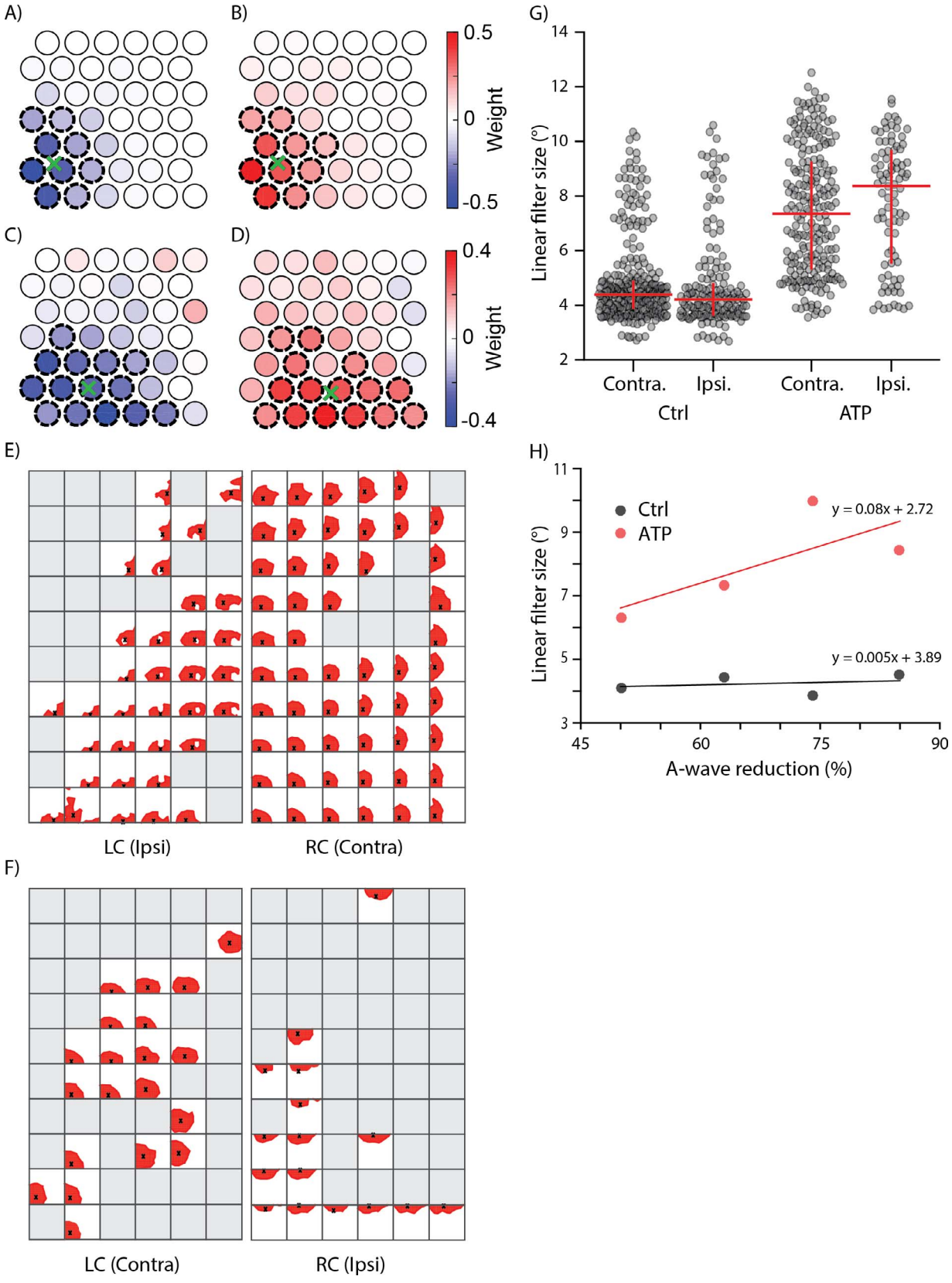

Figure 5. Linear filter (ERF) comparison. (**A**, **B**) Examples of ERFs in response to net anodic-first (**A**) and cathodic-first (**B**) multielectrode stimulation of the control eye. (**C**, **D**) Similar data for stimulation of the ATP-injected eye. *Dotted outlines* indicate significant electrodes, *green crosses* indicate the ERF center. (**E**, **F**) Significant ERF areas for all 120 cortical channels in 15_403B, in response to stimulation of the control eye (**E**) and ATP-injected eye (**F**). *Red* indicates significance, and the center of each ERF is marked with a *black cross*. *Gray sites* are those for which a linear–nonlinear model was not acceptably fitted ($r^2 < 0.5$); they were therefore excluded from ERF analysis. (**G**) ERF sizes (both V_P and V_N) for the control and ATP-injected eyes for well-fitted cortical sites, collated over all experiments (250 of each V_P and V_N for the control eye, 157 of each V_P and V_N for

the ATP-injected eye), split into ipsilateral (ipsi) and contralateral (contra) locations. *Red lines* indicate the medians, first quartile, and third quartile of the linear filter sizes for the healthy and degenerate retinae, collated over all experiments. (**H**) Relationship between the median ERF size and percentage a-wave reduction of the ERG, for the ATP-injected eyes (*red*) with line of best fit. The size of ERFs in the fellow control eyes (*black*) is shown vertically in line with the respective degenerate eye for comparison. LC, left cortex; RC, right cortex.

injected eyes. ERFs were only compared for channels with a correlation coefficient of 0.5 or greater for the fit of the model to the responses (control eye: $n = 163$ contralateral, $n = 87$ ipsilateral; ATP-injected eye: $n = 114$ contralateral, $n = 43$ ipsilateral). ERFs for channels meeting this criterion in 15_403B are shown in Figures 5E and 5F for the healthy retina (87 channels) and degenerate retina (36 channels), respectively. Across the population, distinct differences in ERF size between the healthy and degenerate retinae (Fig. 5G) were found. Specifically, the ERF size in response to stimulation of the ATP-injected eye was significantly larger than for the fellow control eye for both the contralateral and ipsilateral hemispheres (contralateral: $P < 0.001$; ipsilateral: $P < 0.001$, rank sum test), with a larger variance in size. No significant difference in ERF size was evident between different hemispheres when stimulating either retina (healthy: $P = 0.34$; degenerate: $P = 0.20$, rank sum test). In each animal individually, ERFs were also significantly larger in the ATP-injected eye than the fellow control, and a trend was evident between a-wave amplitude reduction and median ERF size across both the contralateral and ipsilateral channels (Fig. 5H). The ERF sizes for the control eyes were not significantly different between experiments ($P > 0.0083$ for all comparisons, rank sum test with Bonferroni correction for six comparisons), while for the degenerate retinae all comparisons were significant ($P < 0.0083$ for all comparisons, rank sum test with Bonferroni correction for six comparisons).

Retinal Degeneration Influences Spatial Extent of Cortical Activation

The ERFs and threshold levels indicate the ability of electrical stimulation of the retina to activate populations of neurons near each cortical channel. Here we quantify and compare the spatial extent and characteristics of cortical activation. Multielectrode stimulation in the healthy retina (Figs. 6A, 6B) and the degenerate retina (Figs. 6C, 6D) typically resulted in responses in both cortical hemispheres, with a stronger contralateral response. However, the response was more widespread and stronger when stimulating the healthy retinae, with multiple scattered peaks of activation. To compare the spatial extent of responses across each recording array for multielectrode stimulation, the spike count measured on each channel was normalized by dividing by the maximum count recorded on that channel. A channel was then considered "active" if its normalized spike rate was greater than three times the standard deviation of the baseline rate. The response size collated over the population, calculated as the percentage of active cortical channels, was larger in the contralateral hemisphere (Fig. 6E) than the ipsilateral hemisphere (Fig. 6F) for both healthy and degenerate retinae ($P < 0.001$, median difference permutation test, with 100,000 samples). In addition, when analyzing each hemisphere separately, responses to stimulation of the healthy retina were on average larger in extent than those from stimulation of the degenerate retina ($P < 0.001$, permutation test for the difference in medians, with 100,000 samples). With the exception of the ipsilateral responses in 15_402B, for which there was no significant difference between eyes ($P = 0.1$), these results were consistent and significant for each animal individually ($P < 0.001$ for all other comparisons).

Discussion

Multielectrode stimulation has shown promise in improving visual outcomes for retinal implant recipients. Previous studies have shown that simultaneous stimulation with multiple electrodes can increase the number of percepts by activating groups of cells between electrodes[14] and increase resolution by inhibiting current spread[15,16] as compared to single-electrode stimulation. However, these studies have involved normally sighted animals, limiting the clinical applicability of their findings. We found that several important differences exist between responses evoked by stimulation of the degenerate eye and normal eye, including response latency, saturated spike rate, activation threshold, ERF size, and cortical spread. While we only performed experiments in a small number of animals with varying levels of degeneration, our results provide support for the hypothesis that the extent of retinal degeneration is the primary underlying reason for the variable results observed in human clinical trials of multielectrode stimulation.

Reduced Response Latency to Multielectrode Stimulation of the Degenerate Retina

The degree of photoreceptor degeneration as measured by a-wave amplitude reduction was less in this cohort as compared to previous work, where at least 70% reduction was reported for all animals at 12 weeks post injection.[24] While this highlights the inherent variability in the ATP-blinding technique, in the present study, sufficient photoreceptor degeneration was classified as at least 50% reduction with accompanying photoreceptor dropout at the area centralis, and all implanted animals met this constraint. There was a difference between the amount of outer retinal thinning overlying the array and the global reduction in photoreceptor function across the four subjects. This is likely due to delay between functional and structural changes, effects of retinal remodeling, and the comparison of a global functional indicator (ERG) versus a localized or regional structural indicator (SD-OCT), since the degeneration is patchy across the retina. However, despite patchiness, all animals exhibited significantly thinned retinae after ATP-induced degeneration. Differences in changes to the inner retina were evident between animals, with one exhibiting thickening, while another showed thinning. These responses are likely due to retinal edema and remodeling, respectively, although eccentricity differences in retinal nerve fiber layer thickness may have a small effect.[36] It has been shown that, in ATP-induced degeneration, the inner retinal layers initially thicken owing to edema/inflammation from the degeneration process, before stabilizing or mildly thinning over time from retinal remodeling.

A significant reduction in response latency to multielectrode stimulation of the degenerate retina was measured in all experiments when compared to single-electrode stimulation or stimulation of the fellow control retina (Fig. 2E). It is possible that these differences were due to the higher total currents delivered to the degenerate retina during multielectrode stimulation.[48–50] The multielectrode stimuli were sampled from Gaussian distributions with standard deviations equal to single electrode P50 currents. These P50 currents were higher

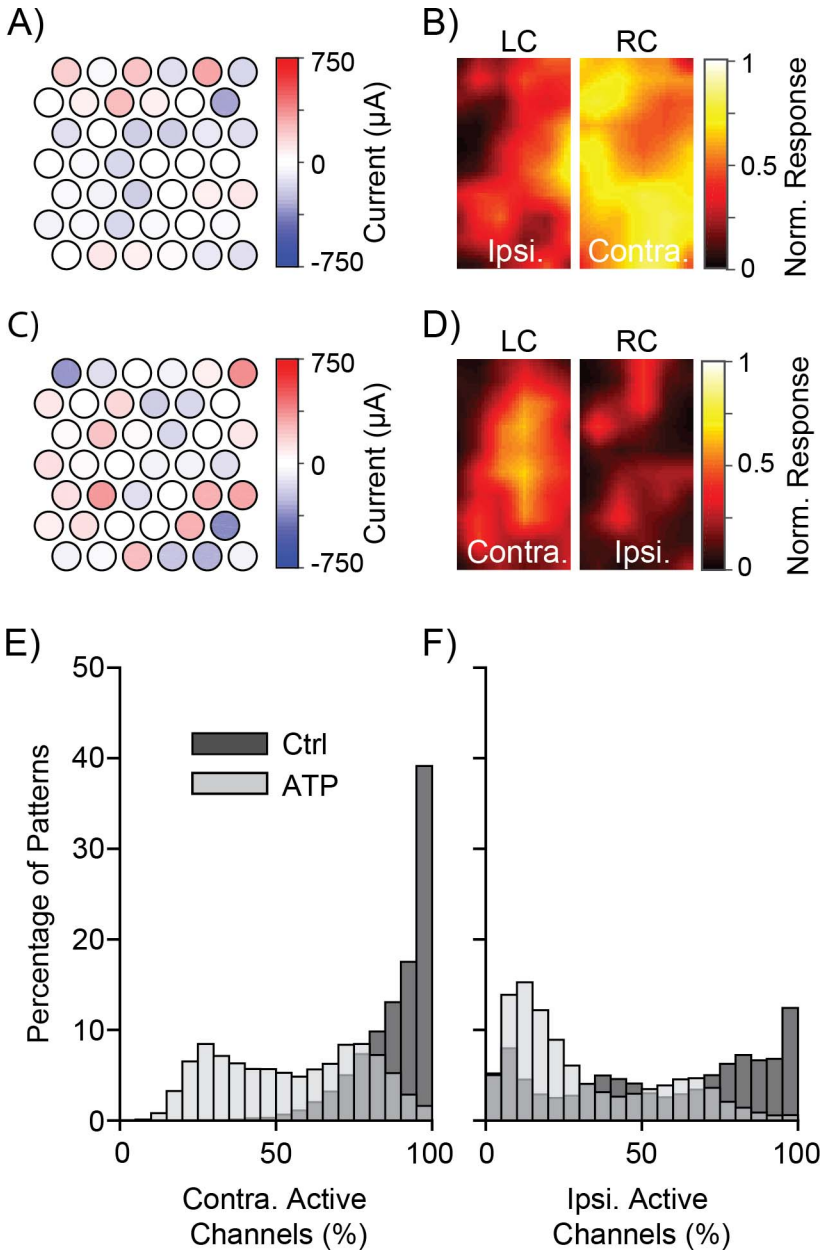

Figure 6. (**A**, **C**) White noise pattern stimuli and (**B**, **D**) resulting cortical responses with spike counts normalized to each channel's own maximum spike count in 15_403B. First row is the stimulus and response of the healthy retina (left eye in this animal, **A** and **B**), second row is the degenerate retina (right eye in this animal, **C** and **D**). For each response, both sides of the cortex are shown: ipsilateral and contralateral to the eye being stimulated. (**E**, **F**) Percentage of channels on the side of cortex contralateral or ipsilateral to the stimulated retina, with a spike count greater than 3 standard deviations of the baseline level, when stimulating the control eye (*dark gray*), as compared to the ATP-injected eye (*light gray*), collated over all animals.

for the ATP-injected retinae, resulting in generally higher multielectrode current amplitudes (standard deviation of multielectrode stimulation over all animals was 191.3 μA for control eye, 247.9 μA for ATP-injected eye). This factor would not influence the latencies seen with single-electrode stimulation, since identical current amplitudes were delivered to both retinae. This is also consistent with a previous study by Aplin et al.,[24] where with single-electrode stimulation no differences in latencies were found between normal and degenerate eye stimulation. However, we also found shorter latencies for single-electrode stimulation of the ATP-injected eye than the control eye in one animal (16_405B). Given that identical stimulation amplitudes were used in both eyes during single-electrode stimulation, this difference likely stems from degeneration of the retina. It is possible that the observed mild thinning of the inner retina seen when using SD-OCT could cause a reduction in response latency by reducing the distance between the electrodes and surviving retinal cells, resulting in more direct activation of RGCs as opposed to mediation through the inner retinal network. However, this can only be confirmed with histologic analysis, which is beyond the scope of this study. Alternatively, changes in signaling pathways during degeneration may have affected the latency of responses. Jensen and Rizzo[51] have reported a reduction in response latency for particular RGC types in rd1 mice retinae compared to those in wild-type retinae in

response to subretinal stimulation, and they suggested that this is possibly due to degeneration preferentially affecting the ON-pathway. Considering the complexity of information pathways within the retina, it is difficult to interpret the exact cause of the latency decrease that we have observed, particularly given that the recording electrodes were far removed and that stimulating from the suprachoroidal space results in extensive current spread. However, these results suggest that further investigation into the temporal characteristics of responses in degenerate retina, particularly with in vitro preparations, is warranted.

These data suggest that the higher charge delivered to the degenerate retina with multielectrode stimulation, possibly coupled with retinal thinning, results in reduced response latency. Since temporal response accuracy may be central to the success of retinal prostheses,[52] the interaction between high overall charge delivered across multiple electrodes simultaneously, and thinned retina due to degeneration, should be considered in future studies.

Nonlinear Response Characteristics Vary With Stimulation and Retina Types

Response thresholds to simultaneous stimulation of multiple electrodes were lower than those seen for single-electrode stimulation for both healthy and degenerate retinae (Figs. 4E, 4F). This is in agreement with clinical,[32,53] preclinical,[39] and modelling[54] studies. The latter shows that multielectrode stimulation from the suprachoroidal space penetrates the retina more effectively than single-electrode stimulation,[54] which could account for the lower thresholds. Previously, increased thresholds in the ATP-injected feline model have been found to correlate with a decrease in retinal ganglion cell density and the extent of retinal gliosis above an electrode.[24] Given that the local degree of degeneration influences threshold, the simultaneous stimulation of multiple electrodes overlying retinal areas with differing degrees of degeneration confounds comparisons to single-electrode responses. Therefore, spatially uneven degeneration or gliosis are possible explanations for the lack of difference in thresholds between the control eye and the ATP-injected eye found in the animal with the lowest percentage a-wave reduction (15_403B). It is unlikely that the large reduction in outer retinal thickness (67%), or thickening of the inner retina in this subject, contributed to the thresholds, since retinal thickness has previously shown no correlation with single-electrode thresholds when stimulating from the suprachoroidal space in cats,[24] or with perceptual thresholds in human patients.[26,55]

Saturated spike rates were found to be higher for multielectrode stimulation than for single-electrode stimulation (Fig. 4C), which is in agreement with a previous in vivo study in normally sighted felines.[39] It is possible that the discrepancy in maximum spike level was due to single-electrode stimulation not actually reaching saturation, and that with higher stimulation amplitudes the spike rate would further increase. However, this is not likely given that the generator current required to reach saturation (P90) was generally similar between stimulus types (Fig. 4D). Therefore, the more likely explanation is that spatial interactions between simultaneously stimulated electrodes activate individual neurons lying intermediately between electrodes that were not activated by single-electrode stimulation alone. This could be further investigated by performing spike sorting to characterize the number of individual neurons exhibiting a response to each stimulus type,[15] but this is outside the scope of this study. Increased spike rates could be the reason for brighter percepts reported by human subjects in response to multielectrode stimulation clinically.[32]

Larger Electrical Receptive Fields and Smaller Activated Area for Stimulation of the Degenerate Retina

Simultaneous stimulation of multiple electrodes results in predominantly linear interactions between the elicited electric fields.[43] The extent over which these interactions occur for a particular cortical location is represented by the size of the ERF associated with that site. Recording channels with linear–nonlinear models that were badly fitted ($r^2 < 0.5$) were excluded from the analysis to ensure that only meaningful ERF sizes were approximated. Stimulation of the ATP-injected eyes was associated with a larger number of badly fitted linear–nonlinear models. This was likely due to the reduced number of channels that were significantly driven by the stimulus, since the model fit is contingent upon the responses recorded on each channel being sufficiently driven by the stimulus. This is also reflected by the reduced spatial area of responses shown for stimulation of the degenerate eye.

We found that ERFs for stimulation of the degenerate retina were significantly larger than for the healthy retina (Fig. 5G). It is unlikely that the size discrepancy was due to different array placements between animals or eyes, given that no differences were found in ERF sizes of healthy retinae between animals. Instead, the increased ERF sizes suggest that, to evoke a cortical response, a larger area of the degenerate retina must be recruited. This is possibly caused by changes in retinal cell excitability and density that occur during degeneration.[19,22,36] In rd10 mice, the excitability of different RGCs has been reported to be variable, with some cells displaying similar thresholds to those in the wild type and others characterized by higher thresholds.[22] If a similar variability in RGC thresholds were to occur in the degenerate feline retina, this could explain the enlarged ERFs. If a larger area of the retina were required to be stimulated to elicit a response at each cortical site, spatially white electrical stimulation (with both anodic-phase first and cathodic-phase first pulses on different electrodes) in the degenerate retina would have a decreased probability of evoking cortical activity, compared to the normal retina, owing to counteracting responses within different retinal neuron populations. Therefore, this agrees with our finding that, in general, stimulation of the degenerate retinae elicits smaller response areas in the cortex than stimulation of the healthy retinae (Fig. 6E). This outcome could not have been predicted from the work of Aplin et al.,[24] who have found that, in the same animal model, selectivity of cortical activity evoked by single-electrode stimulation at threshold is similar between normal and degenerate eyes. Thus, these data highlight the complex interactions that occur with multielectrode stimulation and the need for validation of sophisticated stimulation strategies in animal models exhibiting retinal degeneration.

Our data also suggest that a trend exists between more degeneration and larger ERFs. To further investigate this, the linear–nonlinear model presented here could be used at various intervals over the period of retinal degeneration of a single animal to assess changes in response characteristics with disease progression. Comparing these changes with in vitro investigations of individual cell thresholds at similar time points could help elucidate the physiological mechanisms behind our findings. It is also possible that ERF sizes are mediated by remodeling elsewhere on the visual pathway. Visual deprivation in the form of retinal lesions[56] or rearing with one eye shut[57] has been shown to increase the size of visual receptive fields in the cortex but not the lateral geniculate nucleus. While this was not possible to assess in the current study, changes in retinocortical connections between the ATP-injected and fellow control eyes could be

investigated in future through the injection of tracers to assess the degree of retinocortical remodeling[56,58] and then extraction of the retinae to compare the extent of retinal remodeling. Such a study would also serve to explore the cortical targets of retinal projections. This has been extensively studied in normally sighted felines, showing that most cells located nasally relative to the area centralis project to the contralateral hemisphere. Additionally, some temporally located cells, particularly those close to the area centralis, also project to the contralateral hemisphere.[59–62] Our results suggest that this organization is maintained during degeneration, since, for stimulating arrays located across the vertical midline through the area centralis, contralateral responses were larger by area than ipsilateral for multielectrode stimulation of both degenerate and healthy retinae. However, Aplin et al.[24] have shown that single-electrode stimulation of the degenerate eye elicits larger areas of response in cortex ipsilateral to the degenerate retina. This difference may have been due to the stimulating arrays being located more temporally than those in the present study and, therefore, recruiting a greater number of cells that project to the ipsilateral hemisphere. However, it is also possible that the contrasting results are due to differing drug protocols between studies. In the present study anesthesia was maintained with Propofol, while Methadone was used as an analgesic. However, in the study by Aplin et al.,[24] anesthesia was maintained by using an intravenous infusion of sodium pentobarbitone. Methadone has been found to result in both excitatory and depressive effects on visually evoked potentials recorded in the cortex of the cat,[63] and therefore could also cause differential activation between cortical hemispheres.

The increased ERF sizes affect the applicability of current focusing and steering strategies, particularly if ERFs are also more diffuse, as strategies may require discrete ERF peaks between adjacent electrodes.[15] Application of a linear–nonlinear model as described here and in previous studies[43,44] is a promising avenue not only for identifying response characteristics, but also for optimizing stimulation patterns to shape cortical activity. This could be achieved by fully or partially inverting the model. Full model inversion would involve using a nonlinear optimization algorithm to compute stimulation patterns that would be likely to produce a desired cortical response. Alternatively, a more efficient approach would involve identifying target "responses" in the generator signal subspace, and from here, stimuli associated with these patterns could be retrieved via a linear transformation (multiplication by the pseudoinverse of the linear filter matrix). Shaping cortical responses in this way could improve the efficacy of retinal prostheses.

Conclusion

We showed that significant differences exist between cortical responses to single- and multielectrode stimulation of the healthy and degenerate retina. We showed that multielectrode stimulation in the degenerate retina results in increased retinal penetration and lower thresholds as compared to single-electrode stimulation. This could prove invaluable for prostheses located far from target cells (such as suprachoroidal prostheses) in retinae with already reduced cell counts. However, large ERF sizes may negatively impact the applicability of current focusing and steering strategies. These results highlight that simultaneous stimulation paradigms in trials of normally sighted models do not yield the same results in a degenerate model, and show that a linear–nonlinear model is a useful method of understanding, and possibly harnessing, the complex interactions occurring between simultaneously stimulated electrodes including those continuing to evolve during the progress of retinal degeneration.

Acknowledgments

The authors thank Alexia Saunders, Michelle McPhedran, Alison Neil, Dimitra Stathopoulos, Stephanie Epp, and Ceara McGowan for experimental assistance and animal handling; Owen Burns and Vanessa Maxim for manufacturing of the electrodes; and Thomas Spencer, Ali Almasi, Felix Aplin, Patrick Thien, and Emma Johnson for assistance with data collection.

Supported by a Project Grant from the National Health and Medical Research Council, Australia (GNT No. 1063093). This research was additionally supported by the Australian Research Council through its Special Research Initiative in Bionic Vision Science and Technology awarded to Bionic Vision Australia and the Bertalli Family Foundation to the Bionics Institute. The Bionics Institute and the Centre for Eye Research Australia acknowledge the support they receive from the Victorian Government through its Operational Infrastructure Program. KJH was supported by an Australian Postgraduate Award through the Australian Government and a postgraduate scholarship from the Commonwealth Scientific and Industrial Research Organisation (CSIRO). ANB and YTW acknowledge support under the Australian Research Council's Discovery Projects funding scheme (Project DP140104533).

Disclosure: **K.J. Halupka**, IBM (C), P; **C.J. Abbott**, None; **Y.T. Wong**, None; **S.L. Cloherty**, None; **D.B. Grayden**, P; **A.N. Burkitt**, P; **E.N. Sergeev**, Bionic Vision Australia (C); **C.D. Luu**, None; **A. Brandli**, None; **P.J. Allen**, None; **H. Meffin**, P; **M.N. Shivdasani**, P

References

1. Friedman DS, O'Colmain BJ, Munoz B, et al. Prevalence of age-related macular degeneration in the United States. *Arch Ophthalmol*. 2004;122:564–572.
2. Sharma RK, Ehinger B. Management of hereditary retinal degenerations: present status and future directions. *Surv Ophthalmol*. 1999;43:427–444.
3. Ayton LN, Blamey PJ, Guymer RH, et al. First-in-human trial of a novel suprachoroidal retinal prosthesis. *PLoS One*. 2014;9:e115239.
4. Humayun MS, de Juan E Jr, Dagnelie G, Greenberg RJ, Propst RH, Phillips DH. Visual perception elicited by electrical stimulation of retina in blind humans. *Arch Ophthalmol*. 1996;114:40–46.
5. Zrenner E, Bartz-Schmidt KU, Benav H, et al. Subretinal electronic chips allow blind patients to read letters and combine them to words. *Proc Roy Soc B*. 2011;278:1489–1497.
6. Lewis PM, Ackland HM, Lowery AJ, Rosenfeld JV. Restoration of vision in blind individuals using bionic devices: a review with a focus on cortical visual prostheses. *Brain Res*. 2015;1595:51–73.
7. Barrett JM, Berlinguer-Palmini R, Degenaar P. Optogenetic approaches to retinal prosthesis. *Vis Neurosci*. 2014;31:345–354.
8. Uy H, Chan PS, Cruz FM. Stem cell therapy: a novel approach for vision restoration in retinitis pigmentosa. *Med Hypothesis Discov Innov Ophthalmol J*. 2013;2:52.
9. Rachitskaya AV, Yuan A. Argus II retinal prosthesis system: an update. *Ophthalmic Genet*. 2016;37:1–7.
10. Luo YH-L, da Cruz L. A review and update on the current status of retinal prostheses (bionic eye). *Br Med Bull*. 2014;109:31–44.
11. Stingl K, Bartz-Schmidt KU, Besch D, et al. Subretinal visual implant alpha IMS–clinical trial interim report. *Vision Res*. 2015;111:149–160.

12. Velikay-Parel M, Ivastinovic D, Langmann G, Hornig R, Georgi T, Wedrich A. First experience with The IRIS retinal implant system. *Acta Ophthalmol*. 2009;87:S244.
13. Fujikado T, Kamei M, Sakaguchi H, et al. Testing of semichronically implanted retinal prosthesis by suprachoroidal-transretinal stimulation in patients with retinitis pigmentosa. *Invest Ophthalmol Vis Sci*. 2011;52:4726–4733.
14. Dumm G, Fallon J, Williams C, Shivdasani M. Virtual electrodes by current steering in retinal prostheses. *Invest Ophthalmol Vis Sci*. 2014;55:8077–8085.
15. Jepson L, Hottowy P, Gunning D, et al. Spatially patterned electrical stimulation to enhance resolution of retinal prostheses. *J Neurosci*. 2014;34:4871–4881.
16. Spencer TC, Fallon JB, Thien PC, Shivdasani MN. Spatial restriction of neural activation using focused multipolar stimulation with a retinal prosthesis. *Invest Ophthalmol Vis Sci*. 2016;57:3181–3191.
17. Cicione R, Shivdasani MN, Fallon JB, et al. Visual cortex responses to suprachoroidal electrical stimulation of the retina: effects of electrode return configuration. *J Neural Eng*. 2012;9:036009.
18. Matteucci PB, Chen SC, Tsai D, et al. Current steering in retinal stimulation via a quasimonopolar stimulation paradigm. *Invest Opthalmol Vis Sci*. 2013;54:4307–4320.
19. Chan L, Ray A, Thomas B, Humayun M, Weiland J. In vivo study of response threshold in retinal degenerate model at different degenerate stages. *2008 30th Annual International Conference of the IEEE Engineering in Medicine and Biology Society*. IEEE; 2008:1781–1784.
20. Ye JH, Goo YS. Comparison of voltage parameters for the stimulation of normal and degenerate retina. *2007 29th Annual International Conference of the IEEE Engineering in Medicine and Biology Society*. IEEE; 2007:5782–5785.
21. Suzuki S, Humayun MS, Weiland JD, et al. Comparison of electrical stimulation thresholds in normal and retinal degenerated mouse retina. *Jpn J Ophthalmol*. 2004;48:345–349.
22. Cho A, Ratliff C, Sampath A, Weiland J. Changes in ganglion cell physiology during retinal degeneration influence excitability by prosthetic electrodes. *J Neural Eng*. 2016;13:025001.
23. O'Hearn TM, Sadda SR, Weiland JD, Maia M, Margalit E, Humayun MS. Electrical stimulation in normal and retinal degeneration (rd1) isolated mouse retina. *Vision Res*. 2006;46:3198–3204.
24. Aplin FP, Fletcher EL, Luu CD, et al. Stimulation of a suprachoroidal retinal prosthesis drives cortical responses in a feline model of retinal degeneration. *Invest Ophthalmol Vis Sci*. 2016;57:5216–5229.
25. Rizzo JF, Wyatt J, Loewenstein J, Kelly S, Shire D. Methods and perceptual thresholds for short-term electrical stimulation of human retina with microelectrode arrays. *Invest Ophthalmol Vis Sci*. 2003;44:5355–5361.
26. Shivdasani MN, Sinclair NC, Dimitrov PN, et al. Factors affecting perceptual thresholds in a suprachoroidal retinal prosthesis. *Invest Ophthalmol Vis Sci*. 2014;55:6467–6481.
27. Caspi A, Dorn JD, McClure KH, Humayun MS, Greenberg RJ, McMahon MJ. Feasibility study of a retinal prosthesis: spatial vision with a 16-electrode implant. *Arch Ophthalmol*. 2009;127:398–401.
28. Benav H, Bartz-Schmidt KU, Besch D, et al. Restoration of useful vision up to letter recognition capabilities using subretinal microphotodiodes. *Engineering in Medicine and Biology Society (EMBC), 2010 Annual International Conference of the IEEE*. 2010:5919–5922.
29. Humayun MS, de Juan E Jr, Weiland JD, et al. Pattern electrical stimulation of the human retina. *Vision Res*. 1999;39:2569–2576.
30. Fornos AP, Sommerhalder J, da Cruz L, et al. Temporal properties of visual perception on electrical stimulation of the retina. *Invest Ophthalmol Vis Sci*. 2012;53:2720–2731.
31. Rizzo JF, Wyatt J, Loewenstein J, Kelly S, Shire D. Perceptual efficacy of electrical stimulation of human retina with a microelectrode array during short-term surgical trials. *Invest Ophthalmol Vis Sci*. 2003;44:5362–5369.
32. Horsager A, Greenberg RJ, Fine I. Spatiotemporal interactions in retinal prosthesis subjects. *Invest Ophthalmol Vis Sci*. 2010;51:1223–1233.
33. Freeman DK, Rizzo JF III, Fried SI. Encoding visual information in retinal ganglion cells with prosthetic stimulation. *J Neural Eng*. 2011;8:035005.
34. Hubel DH, Wiesel TN. Early exploration of the visual cortex. *Neuron*. 1998;20:401–412.
35. Aplin FP, Luu CD, Vessey KA, Guymer RH, Shepherd RK, Fletcher EL. ATP-induced photoreceptor death in a feline model of retinal degeneration. *Invest Ophthalmol Vis Sci*. 2014;55:8319–8329.
36. Aplin FP, Vessey KA, Luu CD, Guymer RH, Shepherd RK, Fletcher EL. Retinal changes in an ATP-induced model of retinal degeneration. *Front Neuroanat*. 2016;10:46.
37. Puthussery T, Fletcher E. Extracellular ATP induces retinal photoreceptor apoptosis through activation of purinoceptors in rodents. *J Comp Neurol*. 2009;513:430–440.
38. Vessey KA, Greferath U, Aplin FP, et al. Adenosine triphosphate-induced photoreceptor death and retinal remodeling in rats. *J Comp Neurol*. 2014;522:2928–2950.
39. Shivdasani MN, Fallon JB, Luu CD, et al. Visual cortex responses to single-and simultaneous multiple-electrode stimulation of the retina: implications for retinal prostheses. *Invest Ophthalmol Vis Sci*. 2012;53:6291–6300.
40. Villalobos J, Allen PJ, McCombe MF, et al. Development of a surgical approach for a wide-view suprachoroidal retinal prosthesis: evaluation of implantation trauma. *Graefes Arch Clin Exp Ophthalmol*. 2012;250:399–407.
41. Heffer LF, Fallon JB. A novel stimulus artifact removal technique for high-rate electrical stimulation. *J Neurosci Methods*. 2008;170:277–284.
42. Boinagrov D, Pangratz-Fuehrer S, Goetz G, Palanker D. Selectivity of direct and network-mediated stimulation of the retinal ganglion cells with epi-, sub-and intraretinal electrodes. *J Neural Eng*. 2014;11:026008.
43. Halupka KJ, Shivdasani MN, Cloherty SL, et al. Prediction of cortical responses to simultaneous electrical stimulation of the retina. *J Neural Eng*. 2017;14:016006.
44. Maturana MI, Apollo NV, Hadjinicolaou AE, et al. A simple and accurate model to predict responses to multi-electrode stimulation in the retina. *PLoS Comp Biol*. 2016;12:e1004849.
45. Sekhar S, Jalligampala A, Zrenner E, Rathbun D. Tickling the retina: integration of subthreshold electrical pulses can activate retinal neurons. *J Neural Eng*. 2016;13:046004.
46. Dumoulin SO, Wandell BA. Population receptive field estimates in human visual cortex. *Neuroimage*. 2008;39:647–660.
47. Vakkur G, Bishop P, Kozak W. Visual optics in the cat, including posterior nodal distance and retinal landmarks. *Vision Res*. 1963;3:289–314.
48. Stett A, Barth W, Weiss S, Haemmerle H, Zrenner E. Electrical multisite stimulation of the isolated chicken retina. *Vision Res*. 2000;40:1785–1795.
49. Lee SW, Eddington DK, Fried SI. Responses to pulsatile subretinal electric stimulation: effects of amplitude and duration. *J Neurophysiol*. 2013;109:1954–1968.
50. Tsai D, Morley JW, Suaning GJ, Lovell NH. Direct activation and temporal response properties of rabbit retinal ganglion

Investigative Ophthalmology & Visual Science

cells following subretinal stimulation. *J Neurophysiol*. 2009; 102:2982–2993.

51. Jensen RJ, Rizzo JF III. Activation of retinal ganglion cells in wild-type and rd1 mice through electrical stimulation of the retinal neural network. *Vision Res*. 2008;48:1562–1568.
52. Fried SI, Hsueh H-A, Werblin FS. A method for generating precise temporal patterns of retinal spiking using prosthetic stimulation. *J Neurophysiol*. 2006;95:970–978.
53. Wilke R, Gabel V-P, Sachs H, et al. Spatial resolution and perception of patterns mediated by a subretinal 16-electrode array in patients blinded by hereditary retinal dystrophies. *Invest Ophthalmol Vis Sci*. 2011;52:5995–6003.
54. Wilke R, Moghadam GK, Lovell N, Suaning G, Dokos S. Electric crosstalk impairs spatial resolution of multi-electrode arrays in retinal implants. *J Neural Eng*. 2011;8:046016.
55. de Balthasar C, Patel S, Roy A, et al. Factors affecting perceptual thresholds in epiretinal prostheses. *Invest Ophthalmol Vis Sci*. 2008;49:2303–2314.
56. Darian-Smith C, Gilbert C. Topographic reorganization in the striate cortex of the adult cat and monkey is cortically mediated. *J Neurosci*. 1995;15:1631–1647.
57. Ganz L, Fitch M, Satterberg JA. The selective effect of visual deprivation on receptive field shape determined neurophysiologically. *Exp Neurol*. 1968;22:614–637.
58. Antonini A, Stryker MP. Rapid remodeling of axonal arbors in the visual cortex. *Science*. 1993;260:1819–1821.
59. Tassinari G, Bentivoglio M, Chen S, Campara D. Overlapping ipsilateral and contralateral retinal projections to the lateral geniculate nucleus and superior colliculus in the cat: a retrograde triple labelling study. *Brain Res Bull*. 1997;43: 127–139.
60. Payne B. Neuronal interactions in cat visual cortex mediated by the corpus callosum. *Behav Brain Res*. 1994;64:55–64.
61. Wässle H, Illing RB. The retinal projection to the superior colliculus in the cat: a quantitative study with HRP. *J Comp Neurol*. 1980;190:333–356.
62. Illing RB, Wässle H. The retinal projection to the thalamus in the cat: a quantitative investigation and a comparison with the retinotectal pathway. *J Comp Neurol*. 1981;202:265–285.
63. Snyder E, Shearer D, Dustman R, Beck E. Methadone-induced changes in the visual evoked response recorded from multiple sites in the cat brain. *Psychopharmacology*. 1979;63:89–95.

Investigative Ophthalmology & Visual Science